JACS Au
AN OPEN ACCESS JOURNAL OF THE AMERICAN CHEMICAL SOCIETY

pubs.acs.org/jacsau
Article

Extended Quinolizinium-Fused Corannulene Derivatives: Synthesis and Properties

Lin Huang, Qing Wang, Peng Fu, Yuzhu Sun, Jun Xu, Duncan L. Browne, and Jianhui Huang*

Cite This: JACS Au 2024, 4, 1623−1631
Read Online

ACCESS | Metrics & More | Article Recommendations | Supporting Information

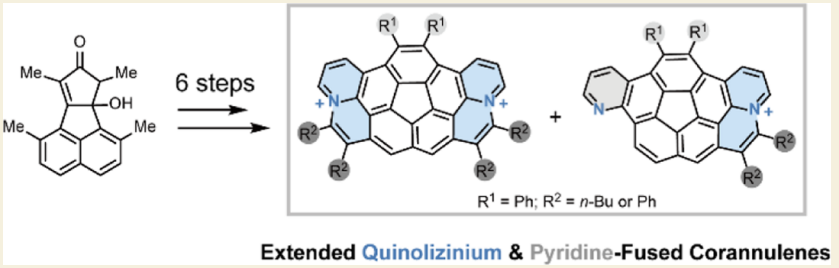

ABSTRACT: Reported here is the design and synthesis of a novel class of extended quinolizinium-fused corannulene derivatives with curved geometry. These intriguing molecules were synthesized through a rationally designed synthetic strategy, utilizing double Skraup−Doebner−Von Miller quinoline synthesis and a rhodium-catalyzed C−H activation/annulation (CHAA) as the key steps. Single-crystal X-ray analysis revealed a bowl depth of 1.28−1.50 Å and a unique "windmill-like" shape packing of **12a**$(2PF_6^-)$ due to the curvature and incorporation of two aminium ions. All of the newly reported curved salts exhibit green to orange fluorescence with enhanced quantum yields (Φ_f = 9−13%) and improved dispersibility compared to the pristine corannulene (Φ_f = 1%). The reduced optical energy gap and lower energy frontier orbital found by doping extended corannulene systems with nitrogen cations was investigated by UV−vis, fluorescence, and theoretical calculations. Electrochemical measurements reveal a greater electron-accepting behavior compared with that of their pyridine analogues. The successful synthesis, isolation, and evaluation of these curved salts provide a fresh perspective and opportunity for the design of cationic nitrogen-doped curved aromatic hydrocarbon-based materials.

KEYWORDS: *nitrogen doped PAHs, corannulene, nitrogen cations, intermolecular packing, photophysical properties*

INTRODUCTION

Curved polycyclic aromatic hydrocarbons (PAHs) have attracted significant attention due to their unique properties.[1−10] Corannulene, with a C_{5v} symmetric and partial fullerene-like structure, is a typical bowl-shaped polycyclic aromatic arene.[11,12] It has unique properties originating from its distorted structure, such as intermolecular packing,[13−15] dynamic inversion behaviors,[16−20] and electron deficiency[21−23] compared with that of classical planar graphene forms. Corannulene derivatives have also been widely applied in research fields such as polymer,[24] organic field effect transistors (OFETs),[25−27] sensors,[28,29] solar cells,[30,31] host−guest chemistry,[32−34] and organic light emitters.[35,36] Doping of heteroatoms into polycyclic aromatic systems is of significant interest, as such heteroatoms can perturb the electronic structures of the original carbon-based compounds and thus offer possibilities for new applications.[37−43] Nonetheless, only limited examples of heteroatom-doped curved systems have been reported, which is in large part hindered by the synthetic challenges of such systems. The most commonly found examples are those with nitrogen atoms at the peripheral positions or within the polycyclic skeleton (Figure 1).[44−52]

The inclusion of pyridinic, pyrrolic, or cationic nitrogen atoms represents a crucial strategy in tuning and inducing distinct electronic effects.[39] Several examples have been synthesized, such as extended π-conjugated azacorannulenes (**1a**, **1b**) bearing a pyrrolic-type nitrogen at the hub position of corannulene core by Shinokubo et al. and Nozaki et al.,[44,45] pyridine-embedded corannulene **2**, with a nitrogen atom at the rim position, by Scott et al.,[46] and peripherally nitrogen-incorporated azaindenocorannulene **3** by Siegel et al.[47] (Figure 1a). Cationic nitrogen-incorporated analogues have been less explored, mainly due to the reactivity and synthetic challenge. Only recently, a cationic corannulene bearing a central imidazolium core was reported by Ito et al. (Figure 1b), showing high water dispersibility and biocompatibility, despite

Received: February 2, 2024
Revised: February 21, 2024
Accepted: February 21, 2024
Published: March 27, 2024

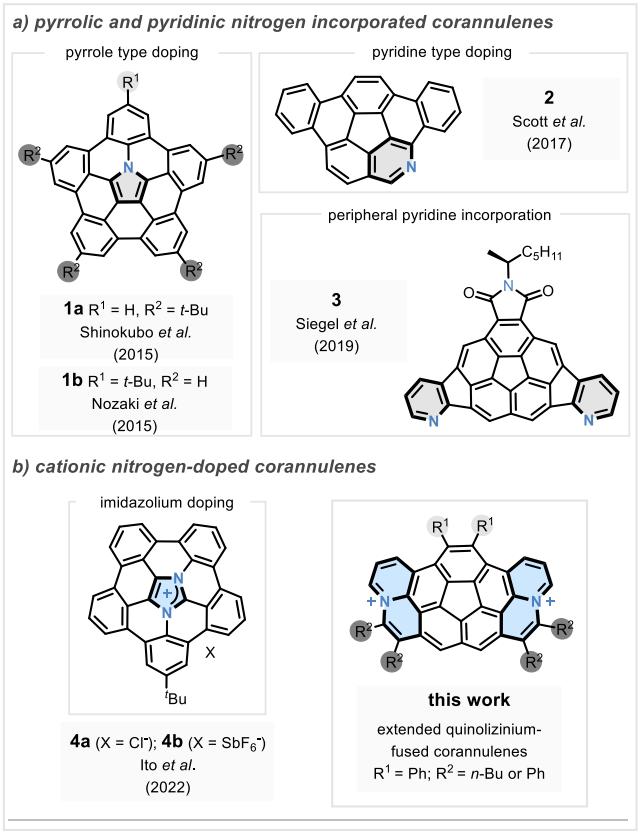

Figure 1. (a) Previous reports on pyrrolic and pyridinic nitrogen-incorporated corannulenes within the polycyclic skeleton (**1a**, **1b**, and **2**) and at the peripheral positions (**3**). (b) Diazapentabenzocorannulenium **4**. (c) Extended quinolizinium-fused corannulenes.

a lack of hydrophilic substituents.[48] Planar cationic nitrogen-doped PAHs have shown interesting photoelectric and self-assembly properties.[53−57] We envisioned that the introduction of curvature may, in combination with cationic nitrogen doping, afford modified optoelectronic properties. Dynamic bowl inversion behavior also provides the possibility of atropisomeric chirality and column-like packing structures.[58] Moreover, the disrupted π-electron delocalization and $\pi-\pi$ interactions of all carbon curved systems will be enhanced by the nitrogen cation doping, which induces a lower band gap and higher electron affinity.[59,60] Herein, we designed and synthesized a novel class of extended corannulene derivatives bearing one (**11a** and **11b**) or two cationic nitrogen atoms (**12a** and **12b**) at the peripheral positions, achieved by a rationally designed synthetic strategy, which includes a double Skraup−Doebner−Von Miller pyridine synthesis and a rhodium-catalyzed C−H activation/annulation (CHAA) reaction as key steps. It was anticipated that these curved π-extended cationic nitrogen-containing PAHs may exhibit interesting structure, properties, and function, compared to their planar analogues.

RESULTS AND DISCUSSION

Design and Synthesis

Our synthetic strategy to extended quinolizinium-fused corannulenes **11a−12b** centered on access to the key intermediate diaminocorannulene **9**, via the regioselective bromination of corannulene **8**. From intermediate **9**, the bilateral construction of pyridine through a double Skraup−Doebner−Von Miller synthesis was envisioned as a prequel to a final transition-metal-catalyzed CHAA process to furnish the cationic quinoline moiety.[61,62] Halocorannulenes have been proven particularly important for the introduction of an amino group through a Pd-catalyzed amination reaction. While some of them, like bromocorannulene, pentachlorocorannulene, and decachlorocorannulene, have been synthesized,[63] dihalogenated-corannulenes have not been extensively studied because of the challenges in controlling the selectivity of halogenation. As illustrated in Scheme 1, to obtain the critical intermediate 4,9-dibromocorannulene **8**, we commenced by adopting the ring-closure method reported by Rabideau and Sygula,[64] Siegel et al.,[65] and Cao et al.[27] using diphenylacetylene as dienophile. Diels−Alder cycloaddition between carbinol **5** and diphenylacetylene in acetic anhydride at 150 °C led to the formation of bisphenyl-substituted tetramethylfluoranthene **6** in a 42% yield after the elimination of a CO molecule. Treatment of **6** with 6 equiv of *N*-bromosuccinimide (NBS) under sun lamp

Scheme 1. Synthetic Route to the Extended Quinolizinium-Fused Corannulenes 11a−12b

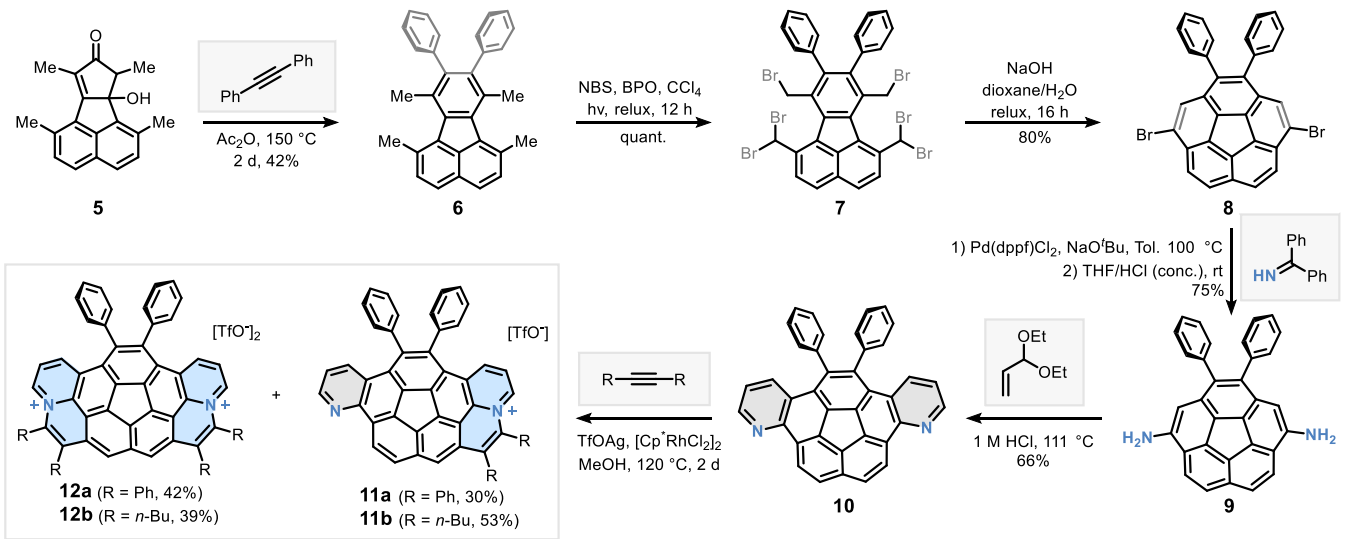

https://doi.org/10.1021/jacsau.4c00105
JACS Au 2024, 4, 1623−1631

irradiation exclusively produced hexabromo-fluoranthene **7**, likely owing to a level of steric control imparted by the phenyl groups. Notably, the use of excess NBS or reaction time can overcome this steric control and lead to overbromination. 4,9-Dibromo-1,2-diphenylcorannulene **8** can be furnished in an 80% yield by heating hexabromo-fluoranthene **7** with sodium hydroxide in dioxane/water (~3:1) to reflux for 16 h.

Efficient and rapid access to π-extended fused heteroaromatics is of great importance in materials science.[40,43,66,67] The synthesis of the crucial second intermediate, dipyridocorannulene **10**, from dibromocorannulene **8** was not straightforward. Diaminocorannulene **9** was synthesized first through a Buchwald–Hartwig amination using benzophenone imine, followed by hydrolysis.[50,68] Subsequently, a double Skraup–Doebner–Von Miller quinoline synthesis,[69] employing acrolein diethylacetal as the reactant in 1 M HCl, was utilized for the preparation of dipyridocorannulene **10** from **9**. Recently, the direct functionalization of C–H bonds in organic compounds has emerged as a potent and optimal approach for generating both carbon–carbon and carbon–heteroatom bonds.[70−72] Based on our continuous research interests in transition-metal-catalyzed CHAA reactions,[73−75] we have attempted the use of palladium, ruthenium, and rhodium catalysts for the final ring closure. The use of both palladium and ruthenium catalysts failed to provide any of the desired product. However, rhodium catalyst[76] Cp^*RhCl_2 afforded the target extended quinolizinium-fused corannulenes successfully. Silver triflate was chosen as the oxidant in this transition, for its efficacy in facilitating the annulation process. This method led to the synthesis of both monoquinolizinium extended corannulenes **11a–b** (30–53%) and bis-quinolizinium extended corannulenes **12a–b** (39–42%) in good yields. Notably, this is the first successful application of a transition-metal-catalyzed CHAA reaction in such a corannulene-based curved π-conjugated system.

X-ray Crystallography

Due to unsuccessful attempts to obtain single crystals of **12a** suitable for X-ray diffraction, an anion metathesis reaction of a solution of **12a** (in acetonitrile) was attempted with potassium hexafluorophosphate (KPF_6) in water to obtain the corresponding hexafluorophosphate salt **12a**$(2PF_6^-)$. Single crystals of **12a**$(2PF_6^-)$ were obtained by the slow evaporation of a toluene/methanol solution at room temperature, which crystallized in the *P*2/*c* space group (Figure 2). The bowl depth, defined as the perpendicular distance from the center of the hub (C1–C5 ring) to the parallel planes containing the carbon atoms C20–C22 and C25–C27 is in the range of 1.28–1.50 Å (Figure 2B). This bowl depth is larger than that of corannulene (0.87 Å),[77] and the curvature of **12a**$(2PF_6^-)$ is further evaluated by Haddon's π-orbital axis vector (POAV)[78,79] angles. As shown in Figure 2A, the POAV angles around the central five-membered ring are in the range of 7.7–8.2°, which are similar to that of corannulene (8.3°).[80] These findings suggest that **12a**$(2PF_6^-)$ has a curvature akin to that of corannulene, yet it exhibits greater depth due to its π-extended architecture. Furthermore, compound **12b**, bearing both *n*-butyl and phenyl substituents, exhibits five distinct split peaks corresponding to the phenyl protons in its ^{1}H NMR spectrum (Figure S32). This phenomenon was not observed in dipyridocorannulene **10**, which has two adjacent phenyl groups and fused pyridine rings (Figure S24). This nonsymmetric feature evidences that the bowl-to-bowl inversion in **12b**

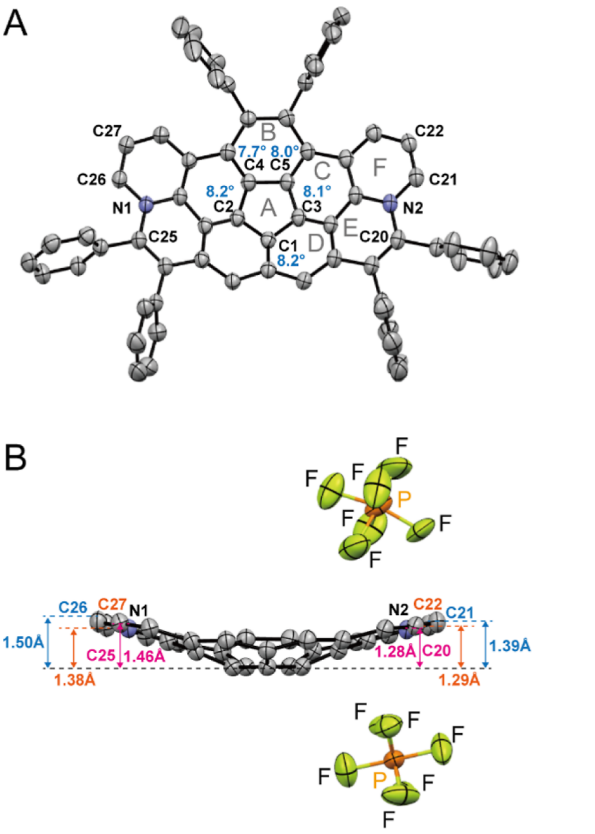

Figure 2. OPTER structure of **12a**$(2PF_6^-)$ with thermal ellipsoids at 45% probability. (A) Top view including POAV angles of C1–C5 (hydrogen atoms and PF_6^- are omitted for clarity). (B) Side view including the calculated bowl depth (hydrogen atoms and phenyl groups have been omitted for clarity).

occurs slower than the NMR timescale at room temperature, indicating a higher inversion energy barrier and a deeper bowl depth, aligning with Siegel's reported correlation between bowl depth and inversion barrier.[20] The inversion barrier was further studied by density functional theory (DFT) calculation at the B3LYP/6-311G (2d, p) level of theory to be 14.0 kcal mol^{-1}, as displayed in Figure 3. This value is larger than that of pristine corannulene (theoretical value: 10.7–11.0 kcal mol^{-1}).[20,81]

The aromaticity of **12a**$(2PF_6^-)$ was evaluated by nucleus-independent chemical shift (NICS) calculations and aniso-

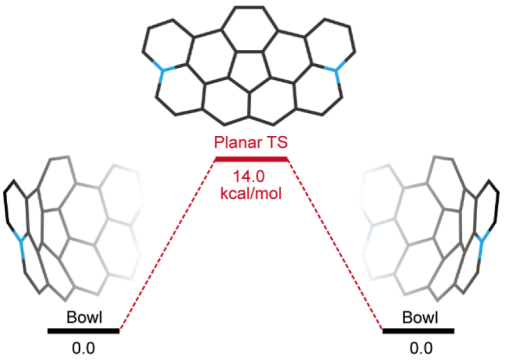

Figure 3. Energy diagram of bowl inversion for **12a**$(2PF_6^-)$ through a planar transition intermediate **TS** (PF_6^- counterions and phenyl groups are omitted for clarity).

https://doi.org/10.1021/jacsau.4c00105
JACS Au 2024, 4, 1623–1631

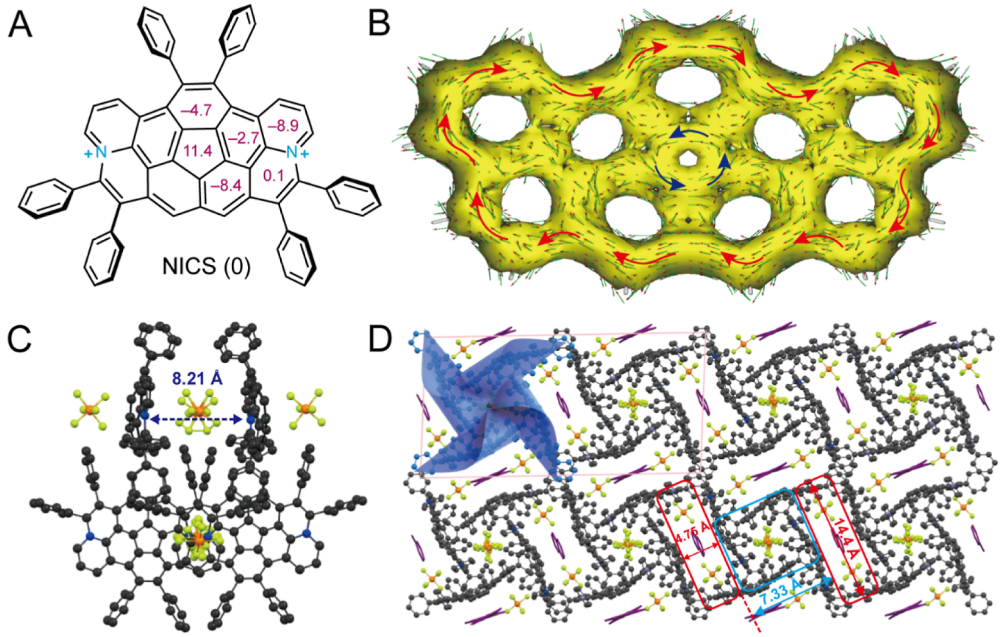

Figure 4. Aromaticity and packing structure of **12a**$(2PF_6^-)$ (ball and stick). (A) NICS (0) values. (B) ACID plot of **12a**$(2PF_6^-)$ (phenyl groups are omitted) by using the AICD 2.0 software. The magnetic field is perpendicular to the molecular plane and points out of the image. The clockwise/anticlockwise circles labeled with red/dark blue arrows indicate the diatropic/paratropic ring current, respectively. (C) Side view of a "windmill-like" unit. Distance between two cationic nitrogen atoms is depicted in deep blue, and solvent molecules (toluene) are omitted for clarity. (D) Packing along the *b*-axis, a blue windmill is superimposed; solvent molecules (toluene) are depicted in purple, and two types of vacant space are depicted in blue and red, respectively.

tropy of the induced current density (ACID) analyses at the B3LYP/6-311G (2d, p) level of theory (Figure 4A, B). A positive NICS (0) value of 11.4 (Figure 4A) and an anticlockwise paratropic ring current (Figure 4B) were predicted for the pentagon (ring A), indicating a localized antiaromaticity of the five-membered ring, which was consistent to that observed for the pristine corannulene. Meanwhile, the NICS (0) of peripheral rings were calculated to be −4.7 (ring B), −2.7 (ring C), and −8.4 (ring D), respectively, suggesting their aromaticity. Interestingly, the NICS (0) values of ring E and ring F, sharing a nitrogen cation dopant, were 0.1 and −8.9, respectively. The opposite values indicated their weak antiaromaticity and aromaticity, respectively. The ACID plot disclosed a distinct clockwise diatropic ring current along the periphery of the whole π-conjugated framework (Figures 4B and S11), indicating a global aromaticity crossed over two quinolizinium motifs.

Interestingly, in these infinite stacks, a distinctive "windmill-like" repeating unit is formed by four **12a**$(2PF_6^-)$ molecules, while the hexafluorophosphate counterions and nitrogen cations align in a linear fashion (Figure 4C,D). In a "windmill-like" unit, four molecules show a *concave/concave* (*cc*/*cc*) packing mode, while between the "windmill-like" units, they are arranged in a *convex/convex* (*cv*/*cv*) manner. This results in the formation of two main types of vacant space within the "windmill-like" and between the "windmill-like" units, depicted in blue and red, respectively (Figure 4D). The distance of the blue space containing hexafluorophosphate is 7.33 Å, and the rectangular red space containing both hexafluorophosphate and solvent toluene molecules has dimensions of 14.4 Å (length) and 4.75 Å (width). The curvature of **12a**$(2PF_6^-)$ leads to unique *cc*/*cc* and *cv*/*cv* stacking, along with the doped cationic nitrogen atoms forming connecting nodes, which give rise to the distinctive "windmill-like" shape crystal structure. It is noteworthy that the solid-state architecture of **12a**$(2PF_6^-)$ is primarily built by the ionic bonds between cationic nitrogen and the PF_6^- counterions. Meanwhile, this special stacking arrangement opens up new possibilities for designing and synthesizing materials with distinctive properties that are seldom achieved in planar structures.[82]

Absorption and Emission Properties

To unravel the impact of both cationic nitrogen dopants and curved π-systems on the overall photophysical properties, UV−vis absorption and fluorescence spectra of compounds **9**−**12b** in CH_2Cl_2 solutions were measured. The results are shown in Figure 5 and Table 1. Extended quinolizinium-fused corannulene derivatives **11a**−**12b** exhibited similar UV−vis absorption maxima at λ = 310−315 nm, situated between that of pristine corannulene (254 nm)[15] and diazapentabenzocorannulenium **4a** (352 nm).[48] Based on the absorption onsets, the optical energy gaps are estimated to range from 2.60 eV (**11a**) and 2.61 eV (**11b**) to 2.43 eV (**12a**) and 2.46 eV (**12b**), which suggests a reduced energy gap of dications (**12a**,**b**) than that of the singly charged derivatives (**11a**,**b**). In the emission spectra, **11a** and **11b** exhibited emission wavelength maxima at λ = 529 and 520 nm compared with the emission wavelength maxima of **12a** and **12b** at λ = 561 and 554 nm, respectively. This result reveals an obvious red shift compared with the emission maxima of corannulene (423 nm) and **4a** (491 nm), which can be attributed to the peripherally π-extended cationic pyridinium/quinolizinium moieties. Notably, a 30 nm red shift was observed between singly charged derivatives (**11a**,**b**) and dications (**12a**,**b**), indicating that the doped cationic nitrogen atom could lower the optical energy gap of such a curved system. As reference, diaminocorannulene **9** displays maximum absorptions at λ = 254 and 294 nm and emission at λ = 521

https://doi.org/10.1021/jacsau.4c00105
JACS Au 2024, 4, 1623−1631

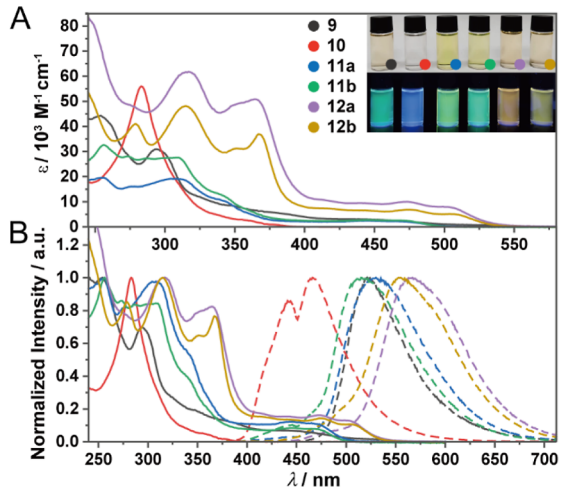

Figure 5. (A) UV−vis absorption spectra of **9**−**12b** in CH_2Cl_2. Inset right: Photographs of their CH_2Cl_2 solutions under visible (top) and UV (365 nm) light (bottom). (B) Normalized absorption (solid lines) and fluorescence (dashed lines) spectra of **9**−**12b** in CH_2Cl_2.

Table 1. Photophysical Properties of 9−12b in CH_2Cl_2[a]

	λ_{abs} (nm)	λ_{em} (nm)[b]	$\lambda_{ex(max)}$ (nm)[c]	SS[d]	Φ_f (%)
9	254, 294	521	305	2.0	31
10	282	443, 467	306	1.4	6
11a	256, 312	529	323	1.3	13
11b	310	520	369	1.3	11
12a	314	561	334	1.4	9
12b	315	554	338	1.4	10

[a]abs = absorption, em = emission, Φ_f = fluorescence quantum yield. [b]λ_{em} was measured with excitation wavelength at 360 nm. [c]$\lambda_{ex(max)}$ = excitation maxima. [d]SS = Stokes shift ($\times 10^4$ cm^{-1}).

nm, which are similar to those of **11a** and **11b**, suggesting that the introduction of two amino groups or a quinolizinium-fused moiety has comparable effects on altering the optical properties of corannulene. Dipyridocorannulene **10** shows UV absorption maxima at λ = 282 nm and emission wavelength maxima at 443 and 467 nm with an obvious blue shift compared with the cationic derivatives. All cationic corannulenes (**11a**−**12b**) have a large Stokes shift range from 1.3 to 1.4 × 10^4 cm^{-1}. The fluorescence quantum yields (Φ_f) in CH_2Cl_2 solutions for these compounds vary from 6 to 31%, with compound **9** demonstrating the largest quantum yield (31%) because of the electron-donating effect of two amino groups. Compared with pristine corannulene, the quinolizinium-fused corannulenes **11a**−**12b** exhibit enhanced solubility in various organic solvents. The incorporation of cationic nitrogen atoms enhances both solubility and fluorescence properties, endowing these curved PAH salts with potential for biological and supramolecular applications.[83]

Electrochemistry

The electrochemical behavior of **10**−**12b** was investigated by cyclic voltammetry (CV) and differential pulse voltammetry (DPV). Measurements were performed in degassed and dry THF using Bu_4NPF_6 as a supporting electrolyte and calibrated versus ferrocenium/ferrocene (Fc^+/Fc). All curves are shown in Figures S4−S9, and the experimental data are summarized in Table S2.

As reference, the pyridine analogue **10** exhibited three reversible reduction waves at −2.21, −2.67, and −2.97 V. In contrast, the extended quinolizinium-fused corannulenes **11a**−**12b** exhibited five reversible reduction waves (Table S2). Upon peripheral π-extension with cationic quinolizinium moieties, the first reduction potentials are significantly increased from **10** (two pyridine moieties, −2.21 V) to **11a**/**11b** (one pyridine and one quinolizinium moiety, −1.09 V/−1.13 V) to **12a**/**12b** (two quinolizinium moieties, −0.88 V/−0.89 V), suggesting a correlation between the reduction potential and the degree of doping with nitrogen cations. The experimental LUMO energy levels of **10**−**12b** were estimated from the onset potentials of the first reduction waves to be −2.65, −3.77, −3.98, −3.72, and −3.97 eV, respectively. Accordingly, their experimental HOMO levels are calculated to be −5.96, −6.37, −6.33, −6.41, and −6.43 eV, respectively, based on the corresponding optical energy gaps. The calculated energies of the HOMO/LUMO level of **10**−**12b** are in good accordance with the experimental data (Table 2).

The effects of doping cationic nitrogen on curved PAHs were further evaluated by DFT calculations at the B3LYP/6-311G (2d, p) level (Table 2 and Figures S12−S17). In comparison to neutral **10**, the HOMO values of singly charged **11a**/**11b** and doubly charged **12a**/**12b** are lowered by 0.43/0.39 eV and 0.88/0.83 eV, and the LUMO values are lowered by 1.32/1.28 eV and 2.08/2.03 eV, respectively, indicating their enhanced electron-accepting properties. The band gaps are also lowered from **10** (4.08 eV) to **11a**−**12b** (2.88−3.19 eV). In addition, the electron-donating *n*-butyl-substituted corannulenes **11b**/**12b** present higher HOMO and LUMO values compared with the parent phenyl substituted corannulenes **11a**/**12a**, which opens the possibility of tuning the electronic nature of such charged π-extended systems.

CONCLUSIONS

In conclusion, we have designed and synthesized four novel π-extended quinolizinium-fused corannulene derivatives **11a,b** and **12a,b** by employing a rationally designed synthetic strategy featuring a double Skraup−Doebner−Von Miller quinoline synthesis and rhodium-catalyzed CHAA as the key

Table 2. Electrochemical Property, Optical Gap, and Theoretical Calculation of Compounds 10−12b

	E_{re} (onset)[a]	E_{LUMO}[b] (eV)	E_{HOMO}[c] (eV)	optical gap[d] (eV)	LUMO[e] (eV)	HOMO[e] (eV)	HOMO−LUMO gap[e] (eV)
10	−2.15	−2.65	−5.96	3.31	−2.19	−6.27	4.08
11a	−1.03	−3.77	−6.37	2.60	−3.51	−6.70	3.19
11b	−1.08	−3.72	−6.33	2.61	−3.47	−6.66	3.18
12a	−0.82	−3.98	−6.41	2.43	−4.27	−7.15	2.88
12b	−0.83	−3.97	−6.43	2.46	−4.22	−7.10	2.89

[a]Onset value of the first reduction potentials obtained from CV. [b]The LUMO energy was calculated using the relation $E_{LUMO} = -(E_{re(onset)}$ vs Fc/Fc^+ + 4.8) eV. [c]HOMO was estimated according to $E_{HOMO} = E_{LUMO} + E_g$. [d]Optical gap ($E_g$) was estimated from the UV−vis onset value. [e]Obtained from theoretical calculations at the B3LYP/6-311G (2d, p) level of theory.

https://doi.org/10.1021/jacsau.4c00105
JACS Au 2024, 4, 1623−1631

steps. In the solid state, the obtained **12a**($2PF_6^-$) exhibits an extended discoidal structure with an inversion barrier of 14.0 kcal/mol, which was confirmed by DFT calculations. Meanwhile, it stacks with a unique "windmill-like" repeating unit that is unusual compared to the packing behaviors of planar forms. Furthermore, UV−vis and fluorescence spectra reveal their enhanced fluorescence efficiency and large Stokes shift. Upon peripheral π-extension with cationic quinolizinium moieties, lower band gaps and higher electron affinity are introduced, implying their potential as (opto)electronic materials. In this work, the charged corannulene-based curved topology lays the foundation for the future construction of curved cationic nitrogen-doped nanocarbon materials.

METHODS

General Information

Unless otherwise stated, all chemicals were of reagent grade or higher, obtained from commercial sources, and used without further purification. Flash chromatography was performed on silica gel 200−300 mesh or neutral Al_2O_3. Thin layer chromatography (TLC) was performed on glass-backed plates precoated with silica (GF254), which were developed using standard visualizing agents. ^1H and ^{13}C NMR spectra were recorded on a 400 or 600 MHz Bruker AVANCE spectrometer at 298 K. Chemical shifts (δ) are reported in ppm with the solvent resonance as the internal standard ($CDCl_3$ ^1H: δ 7.26, ^{13}C: δ 77.16). Data are reported as follows: chemical shift, multiplicity (s = singlet, d = doublet, t = triplet, q = quartet, br = broad, m = multiplet), integration, and coupling constants (J) in Hz. IR absorption spectra were recorded using a Bruker Tensor II FTIR spectrometer (MCT detector, 4000−400 cm^{-1} range, resolution of 4 cm^{-1}, averaging by 16 scans). Melting points were recorded on a national standard melting point apparatus without correction. High-resolution mass spectra (HRMS) were recorded for accurate mass analysis on a Q-TOF micro (Bruker Compass Data Analysis 4.0) spectrometer.

Photophysical and Electrochemical Methods

The UV absorption spectra were measured with an Agilent Cary 60 UV−vis spectrophotometer. Fluorescence excitation/emission measurements were carried out on an Edinburgh FLS980 spectrophotometer, using a 450 W xenon arc lamp, with excitation and emission slit widths at 1 nm. Absolute quantum yields were measured using an integrating sphere detector from Edinburgh Instruments. CV and DPV curves were recorded on a Shanghai Chenhua Instrument Co. Ltd. CHI660E Electrochemical Workstation.

X-ray Diffraction

A single crystal with dimensions 0.03 mm × 0.03 mm × 0.05 mm was selected and mounted in inert oil and then transferred to the cold gas stream of a Rigaku XtaLAB FRX diffractometer equipped with the Hypix6000HE detector. X-ray diffraction intensity data were recorded using mirror-focused Cu Kα radiation (λ = 1.54184 Å) and reduced by using the software package CrysAlisPro, applying an empirical absorption correction. The structure was solved by the intrinsic phasing method using the SHELXT[84] structure solution program and then refined with the SHELXL[84] refinement package using least-squares minimization in OLEX2.[85]

DFT Calculations

The computations were performed by using the Gaussian 16 (revision B.01) program[86] by the B3LYP method with the 6-311G (2d, p) basis set for structure optimization, energy calculations (the counteranions were deleted and the solvation model was used with tetrahydrofuran), NICS,[87] and ACID[88] calculations. The geometry of planar **TS** was optimized without symmetry assumption, and IRC calculations were also performed to check the transition states.

ASSOCIATED CONTENT

Supporting Information

The Supporting Information is available free of charge at https://pubs.acs.org/doi/10.1021/jacsau.4c00105.

Details of the synthesis and spectroscopic characterization of new compounds (PDF)

Crystallographic data (CCDC no.: 2326727), theoretical calculation, and electrochemical data (CIF)

AUTHOR INFORMATION

Corresponding Author

Jianhui Huang − *School of Pharmaceutical Science and Technology, Tianjin University, Tianjin 300072, P. R. China; Collaborative Innovation Center of Chemical Science and Engineering (Tianjin), Tianjin 300072, P. R. China; Tianjin Key Laboratory for Modern Drug Delivery & High-Efficiency, School of Pharmaceutical Science and Technology, Tianjin University, Tianjin 300072, P. R. China;* orcid.org/0000-0001-7281-663X; Email: jhuang@tju.edu.cn

Authors

Lin Huang − *School of Pharmaceutical Science and Technology, Tianjin University, Tianjin 300072, P. R. China; Collaborative Innovation Center of Chemical Science and Engineering (Tianjin), Tianjin 300072, P. R. China; Tianjin Key Laboratory for Modern Drug Delivery & High-Efficiency, School of Pharmaceutical Science and Technology, Tianjin University, Tianjin 300072, P. R. China*

Qing Wang − *School of Pharmaceutical Science and Technology, Tianjin University, Tianjin 300072, P. R. China; National Institute of Biological Sciences, Beijing, Beijing 102206, China;* orcid.org/0000-0002-1155-2340

Peng Fu − *School of Pharmaceutical Science and Technology, Tianjin University, Tianjin 300072, P. R. China; Collaborative Innovation Center of Chemical Science and Engineering (Tianjin), Tianjin 300072, P. R. China; Tianjin Key Laboratory for Modern Drug Delivery & High-Efficiency, School of Pharmaceutical Science and Technology, Tianjin University, Tianjin 300072, P. R. China*

Yuzhu Sun − *School of Pharmaceutical Science and Technology, Tianjin University, Tianjin 300072, P. R. China; Collaborative Innovation Center of Chemical Science and Engineering (Tianjin), Tianjin 300072, P. R. China; Tianjin Key Laboratory for Modern Drug Delivery & High-Efficiency, School of Pharmaceutical Science and Technology, Tianjin University, Tianjin 300072, P. R. China*

Jun Xu − *School of Pharmaceutical Science and Technology, Tianjin University, Tianjin 300072, P. R. China;* orcid.org/0000-0002-2562-2872

Duncan L. Browne − *Department of Pharmaceutical and Biological Chemistry, School of Pharmacy, University College London (UCL), Bloomsbury, London WC1N 1AX, U.K.;* orcid.org/0000-0002-8604-229X

Complete contact information is available at: https://pubs.acs.org/10.1021/jacsau.4c00105

Author Contributions

L.H. and J.H. conceived of the project. L.H. performed the experiments and data analysis. Q.W. executed all the theoretical calculations. P.F. performed the synthetic experiments. Y.S. analyzed the photophysical data. J.X. solved and

https://doi.org/10.1021/jacsau.4c00105
JACS Au 2024, 4, 1623−1631

refined the X-ray structures. L.H. wrote the original manuscript. D.L.B. and J.H. revised and edited the manuscript. J.H. acquired funding and supervised the project. All authors have given approval to the final version of the manuscript.

Notes

The authors declare no competing financial interest.

■ ACKNOWLEDGMENTS

The authors are grateful for the funding support from the National Program on the Key Basic Research Project of China (973 Program) (2015CB856500) and the National Natural Science Foundation of China (NSFC) (grant nos. 21672159 and 21871207). The Instrumental Analysis Center of SPST at Tianjin University is acknowledged for providing NMR, HRMS, and X-ray crystal diffraction analysis. The authors are further thankful to Andrew C. -H. Sue and Jay S. Siegel for their constructive comments and suggestions.

■ REFERENCES

(1) Tsefrikas, V. M.; Scott, L. T. Geodesic Polyarenes by Flash Vacuum Pyrolysis. *Chem. Rev.* **2006**, *106*, 4868−4884.
(2) Wu, Y. T.; Siegel, J. S. Aromatic Molecular-Bowl Hydrocarbons: Synthetic Derivatives, Their Structures, and Physical Properties. *Chem. Rev.* **2006**, *106*, 4843−4867.
(3) Baldridge, K. K.; Siegel, J. S. Of Graphs and Graphenes: Molecular Design and Chemical Studies of Aromatic Compounds. *Angew. Chem., Int. Ed.* **2013**, *52*, 5436−5438.
(4) Liu, L.; Liu, F.; Zhao, J. Curved Carbon Nanotubes: From Unique Geometries to Novel Properties and Peculiar Applications. *Nano Res.* **2014**, *7*, 626−657.
(5) Dutta, A. K.; Linden, A.; Zoppi, L.; Baldridge, K. K.; Siegel, J. S. Extended Corannulenes: Aromatic Bowl/Sheet Hybridization. *Angew. Chem., Int. Ed.* **2015**, *54*, 10792−10796.
(6) Rickhaus, M.; Mayor, M.; Juríček, M. Chirality in Curved Polyaromatic Systems. *Chem. Soc. Rev.* **2017**, *46*, 1643−1660.
(7) Zhang, Q.; Kawasumi, K.; Segawa, Y.; Itami, K.; Scott, L. T. Palladium-Catalyzed C-H Activation Taken to the Limit. Flattening an Aromatic Bowl by Total Arylation. *J. Am. Chem. Soc.* **2012**, *134*, 15664−15667.
(8) Matsubara, S.; Koga, Y.; Segawa, Y.; Murakami, K.; Itami, K. Creation of Negatively Curved Polyaromatics Enabled by Annulative Coupling That Forms an Eight-Membered Ring. *Nat. Catal.* **2020**, *3*, 710−718.
(9) Xie, S. Y.; Gao, F.; Lu, X.; Huang, R. B.; Wang, C. R.; Zhang, X.; Liu, M. L.; Deng, S. L.; Zheng, L. S. Capturing the Labile Fullerene[50] as $C_{50}H_{10}$. *Science* **2004**, *304*, 699.
(10) Brenner, W.; Ronson, T. K.; Nitschke, J. R. Separation and Selective Formation of Fullerene Adducts within an $M^{II}_8L_6$ Cage. *J. Am. Chem. Soc.* **2017**, *139*, 75−78.
(11) Nestoros, E.; Stuparu, M. C. Corannulene: A Molecular Bowl of Carbon with Multifaceted Properties and Diverse Applications. *Chem. Commun.* **2018**, *54*, 6503−6519.
(12) Stuparu, M. C. Corannulene: A Curved Polyarene Building Block for the Construction of Functional Materials. *Acc. Chem. Res.* **2021**, *54*, 2858−2870.
(13) Guo, T.; Li, A.; Xu, J.; Baldridge, K. K.; Siegel, J. Enantiopure C_5 Pentaindenocorannulenes: Chiral Graphenoid Materials. *Angew. Chem., Int. Ed.* **2021**, *60*, 25809−25814.
(14) Tian, X.; Xu, J.; Baldridge, K. K.; Siegel, J. S. Fluorous Corannulenes: Ab Initio Predictions and the Synthesis of Sym-Pentafluorocorannulene. *Angew. Chem., Int. Ed.* **2020**, *59*, 1460−1464.
(15) Wu, Y. T.; Bandera, D.; Maag, R.; Linden, A.; Baldridge, K. K.; Siegel, J. S. Multiethynyl Corannulenes: Synthesis, Structure, and Properties. *J. Am. Chem. Soc.* **2008**, *130*, 10729−10739.
(16) Borchardt, A.; Fuchicello, A.; Kilway, K. V.; Baldridge, K. K.; Siegel, J. S. Synthesis and Dynamics of the Corannulene Nucleus. *J. Am. Chem. Soc.* **1992**, *114*, 1921−1923.
(17) Scott, L. T. H.; Hashemi, M. M.; Bratcher, M. S. Corannulene bowl-to-bowl inversion is rapid at room temperature. *J. Am. Chem. Soc.* **1992**, *114*, 1920−1921.
(18) Seiders, T. J.; Baldridge, K. K.; Elliott, E. L.; Grube, G. H.; Siegel, J. S. Synthesis and Quantum Mechanical Structure of Sym-Pentamethylcorannulene and Decamethylcorannulene. *J. Am. Chem. Soc.* **1999**, *121*, 7439−7440.
(19) Juríček, M.; Strutt, N. L.; Barnes, J. C.; Butterfield, A. M.; Dale, E. J.; Baldridge, K. K.; Stoddart, J. F.; Siegel, J. S. Induced-Fit Catalysis of Corannulene Bowl-to-Bowl Inversion. *Nat. Chem.* **2014**, *6*, 222−228.
(20) Seiders, T. J.; Baldridge, K. K.; Grube, G. H.; Siegel, J. S. Structure/Energy Correlation of Bowl Depth and Inversion Barrier in Corannulene Derivatives: Combined Experimental and Quantum Mechanical Analysis. *J. Am. Chem. Soc.* **2001**, *123*, 517−525.
(21) Ayalon, A.; Rabinovitz, M.; Cheng, P.-C.; Scott, L. T. Corannulene Tetraanion: A Novel Species with Concentric Anionic Rings. *Angew. Chem., Int. Ed.* **1992**, *31*, 1636−1637.
(22) Zabula, A. V.; Filatov, A. S.; Spisak, S. N.; Rogachev, A. Y.; Petrukhina, M. A. A Main Group Metal Sandwich: Five Lithium Cations Jammed between Two Corannulene Tetraanion Decks. *Science* **2011**, *333*, 1008−1011.
(23) Ayalon, A.; Sygula, A.; Cheng, P. C.; Rabinovitz, M.; Rabideau, P. W.; Scott, L. T. Stable High-Order Molecular Sandwiches: Hydrocarbon Polyanion Pairs with Multiple Lithium Ions inside and Out. *Science* **1994**, *265*, 1065−1067.
(24) Stuparu, M. C. Rationally Designed Polymer Hosts of Fullerene. *Angew. Chem., Int. Ed.* **2013**, *52*, 7786−7790.
(25) Shi, K.; Lei, T.; Wang, X.-Y.; Wang, J.-Y.; Pei, J. A Bowl-Shaped Molecule for Organic Field-Effect Transistors: Crystal Engineering and Charge Transport Switching by Oxygen Doping. *Chem. Sci.* **2014**, *5*, 1041−1045.
(26) Lu, R. Q.; Zhou, Y. N.; Yan, X. Y.; Shi, K.; Zheng, Y. Q.; Luo, M.; Wang, X. C.; Pei, J.; Xia, H.; Zoppi, L.; Baldridge, K. K.; Siegel, J. S.; Cao, X. Y. Thiophene-Fused Bowl-Shaped Polycyclic Aromatics with a Dibenzo[*a*,*g*]Corannulene Core for Organic Field-Effect Transistors. *Chem. Commun.* **2015**, *51*, 1681−1684.
(27) Lu, R.-Q.; Xuan, W.; Zheng, Y.-Q.; Zhou, Y.-N.; Yan, X.-Y.; Dou, J.-H.; Chen, R.; Pei, J.; Weng, W.; Cao, X.-Y. A Corannulene-Based Donor-Acceptor Polymer for Organic Field-Effect Transistors. *RSC Adv.* **2014**, *4*, 56749−56755.
(28) Niamnont, N.; Kimpitak, N.; Wongravee, K.; Rashatasakhon, P.; Baldridge, K. K.; Siegel, J. S.; Sukwattanasinitt, M. Tunable Star-Shaped Triphenylamine Fluorophores for Fluorescence Quenching Detection and Identification of Nitro-Aromatic Explosives. *Chem. Commun.* **2013**, *49*, 780−782.
(29) Wu, D.; Shao, T.; Men, J.; Chen, X.; Gao, G. Superaromatic Terpyridines Based on Corannulene Responsive to Metal Ions. *Dalton Trans.* **2014**, *43*, 1753−1761.
(30) Lu, R.-Q.; Zheng, Y.-Q.; Zhou, Y.-N.; Yan, X.-Y.; Lei, T.; Shi, K.; Zhou, Y.; Pei, J.; Zoppi, L.; Baldridge, K. K.; Siegel, J. S.; Cao, X.-Y. Corannulene Derivatives as Non-Fullerene Acceptors in Solution-Processed Bulk Heterojunction Solar Cells. *J. Mater. Chem. A* **2014**, *2*, 20515−20519.
(31) An, M.-W.; Wu, B.-S.; Wang, S.; Chen, Z.-C.; Su, Y.; Deng, L.-L.; Li, S.-H.; Nan, Z.-A.; Tian, H.-R.; Liu, X.-L.; Yun, D.-Q.; Zhang, Q.; Xie, S.-Y.; Zheng, L.-S. Corannulene-Based Hole-Transporting Material for Efficient and Stable Perovskite Solar Cells. *Cell Rep. Phys. Sci.* **2021**, *2*, 100662.
(32) Ronson, T. K.; Wang, Y.; Baldridge, K.; Siegel, J. S.; Nitschke, J. R. An S_{10}-Symmetric 5-Fold Interlocked [2]Catenane. *J. Am. Chem. Soc.* **2020**, *142*, 10267−10272.
(33) Zhang, D.; Ronson, T. K.; Lavendomme, R.; Nitschke, J. R. Selective Separation of Polyaromatic Hydrocarbons by Phase Transfer of Coordination Cages. *J. Am. Chem. Soc.* **2019**, *141*, 18949−18953.

https://doi.org/10.1021/jacsau.4c00105
JACS Au 2024, 4, 1623−1631

(34) Xu, Y. Y.; Tian, H. R.; Li, S. H.; Chen, Z. C.; Yao, Y. R.; Wang, S. S.; Zhang, X.; Zhu, Z. Z.; Deng, S. L.; Zhang, Q.; Yang, S.; Xie, S. Y.; Huang, R. B.; Zheng, L. S. Flexible Decapyrrylcorannulene Hosts. *Nat. Commun.* **2019**, *10*, 485.
(35) Mack, J.; Vogel, P.; Jones, D.; Kaval, N.; Sutton, A. The Development of Corannulene-Based Blue Emitters. *Org. Biomol. Chem.* **2007**, *5*, 2448−2452.
(36) Valenti, G.; Bruno, C.; Rapino, S.; Fiorani, A.; Jackson, E. A.; Scott, L. T.; Paolucci, F.; Marcaccio, M. Intense and Tunable Electrochemiluminescence of Corannulene. *J. Phys. Chem. C* **2010**, *114*, 19467−19472.
(37) Jiang, W.; Li, Y.; Wang, Z. Heteroarenes as High Performance Organic Semiconductors. *Chem. Soc. Rev.* **2013**, *42*, 6113−6127.
(38) Wang, X.; Sun, G.; Routh, P.; Kim, D. H.; Huang, W.; Chen, P. Heteroatom-Doped Graphene Materials: Syntheses, Properties and Applications. *Chem. Soc. Rev.* **2014**, *43*, 7067−7098.
(39) Narita, A.; Wang, X. Y.; Feng, X.; Müllen, K. New Advances in Nanographene Chemistry. *Chem. Soc. Rev.* **2015**, *44*, 6616−6643.
(40) Stępień, M.; Gońka, E.; Żyła, M.; Sprutta, N. Heterocyclic Nanographenes and Other Polycyclic Heteroaromatic Compounds: Synthetic Routes, Properties, and Applications. *Chem. Rev.* **2017**, *117*, 3479−3716.
(41) Wu, Y. F.; Ying, S. W.; Liao, S. D.; Zhang, L.; Du, J. J.; Chen, B. W.; Tian, H. R.; Xie, F. F.; Xu, H.; Deng, S. L.; Zhang, Q.; Xie, S. Y.; Zheng, L. S. Sulfur-Doped Quintuple [9]Helicene with Azacorannulene as Core. *Angew. Chem.* **2022**, *134*, No. e202204334.
(42) Wu, Y. F.; Ying, S. W.; Su, L. Y.; Du, J. J.; Zhang, L.; Chen, B. W.; Tian, H. R.; Xu, H.; Zhang, M. L.; Yan, X.; Zhang, Q.; Xie, S. Y.; Zheng, L. S. Nitrogen-Embedded Quintuple [7]Helicene: A Helicene-Azacorannulene Hybrid with Strong near-Infrared Fluorescence. *J. Am. Chem. Soc.* **2022**, *144*, 10736−10742.
(43) Borissov, A.; Maurya, Y. K.; Moshniaha, L.; Wong, W.-S.; Żyła-Karwowska, M.; Stępień, M. Recent Advances in Heterocyclic Nanographenes and Other Polycyclic Heteroaromatic Compounds. *Chem. Rev.* **2022**, *122*, 565−788.
(44) Ito, S.; Tokimaru, Y.; Nozaki, K. Benzene-Fused Azacorannulene Bearing an Internal Nitrogen Atom. *Angew. Chem., Int. Ed.* **2015**, *54*, 7256−7260.
(45) Yokoi, H.; Hiraoka, Y.; Hiroto, S.; Sakamaki, D.; Seki, S.; Shinokubo, H. Nitrogen-Embedded Buckybowl and Its Assembly with C_{60}. *Nat. Commun.* **2015**, *6*, 8215.
(46) Tsefrikas, V. M.; Greene, A. K.; Scott, L. T. 5-Azadibenzo-[a,G]Corannulene. *Org. Chem. Front.* **2017**, *4*, 688−698.
(47) Tian, X.; Roch, L. M.; Vanthuyne, N.; Xu, J.; Baldridge, K. K.; Siegel, J. S. Azaindenocorannulenes: Synthesis, Properties, and Chirality. *Org. Lett.* **2019**, *21*, 3510−3513.
(48) Li, Q. Q.; Hamamoto, Y.; Kwek, G.; Xing, B.; Li, Y.; Ito, S. Diazapentabenzocorannulenium: A Hydrophilic/Biophilic Cationic Buckybowl. *Angew. Chem., Int. Ed.* **2022**, *61*, No. e202112638.
(49) Tokimaru, Y.; Ito, S.; Nozaki, K. A Hybrid of Corannulene and Azacorannulene: Synthesis of a Highly Curved Nitrogen-Containing Buckybowl. *Angew. Chem., Int. Ed.* **2018**, *57*, 9818−9822.
(50) Ghosh, A.; Csókás, D.; Budanović, M.; Webster, R. D.; Pápai, I.; Stuparu, M. C. Synthesis of Azahelicenes through Mallory Reaction of Imine Precursors: Corannulene Substrates Provide an Exception to the Rule in Oxidative Photocyclizations of Diarylethenes. *Chem. Sci.* **2021**, *12*, 3977−3983.
(51) Kise, K.; Ooi, S.; Saito, H.; Yorimitsu, H.; Osuka, A.; Tanaka, T. Five-Fold Symmetric Pentaindolo- and Pentakis(Benzoindolo)-Corannulenes: Unique Structural Dynamics Derived from the Combination of Helical and Bowl Inversions. *Angew. Chem., Int. Ed.* **2021**, *61*, No. e202112589.
(52) Nakamura, K.; Ochiai, K.; Yubuta, A.; He, D.; Miyajima, D.; Ito, S. Pyridine-Fused Azacorannulene: Fine-Tuning of the Structure and Properties of Nitrogen-Embedded Buckybowls. *Precis. Chem.* **2023**, *1*, 29−33.
(53) Wu, D.; Pisula, W.; Enkelmann, V.; Feng, X.; Müllen, K. Controllable Columnar Organization of Positively Charged Polycyclic Aromatic Hydrocarbons by Choice of Counterions. *J. Am. Chem. Soc.* **2009**, *131*, 9620−9621.
(54) Wu, D.; Zhi, L.; Bodwell, G. J.; Cui, G.; Tsao, N.; Müllen, K. Self-Assembly of Positively Charged Discotic Pahs: From Nanofibers to Nanotubes. *Angew. Chem., Int. Ed.* **2007**, *46*, 5417−5420.
(55) Mali, K. S.; Wu, D.; Feng, X.; Müllen, K.; Van der Auweraer, M.; De Feyter, S. Scanning Tunneling Microscopy-Induced Reversible Phase Transformation in the Two-Dimensional Crystal of a Positively Charged Discotic Polycyclic Aromatic Hydrocarbon. *J. Am. Chem. Soc.* **2011**, *133*, 5686−5688.
(56) Wu, D.; Liu, R.; Pisula, W.; Feng, X.; Müllen, K. Two-Dimensional Nanostructures from Positively Charged Polycyclic Aromatic Hydrocarbons. *Angew. Chem., Int. Ed.* **2011**, *50*, 2791−2794.
(57) Berger, R.; Giannakopoulos, A.; Ravat, P.; Wagner, M.; Beljonne, D.; Feng, X.; Müllen, K. Synthesis of Nitrogen-Doped Zigzag-Edge Peripheries: Dibenzo-9a-Azaphenalene as Repeating Unit. *Angew. Chem., Int. Ed.* **2014**, *53*, 10520−10524.
(58) Wang, Y.; Allemann, O.; Balaban, T. S.; Vanthuyne, N.; Linden, A.; Baldridge, K. K.; Siegel, J. S. Chiral Atropisomeric Indenocorannulene Bowls: Critique of the Cahn-Ingold-Prelog Conception of Molecular Chirality. *Angew. Chem., Int. Ed.* **2018**, *57*, 6470−6474.
(59) Wang, H.; Maiyalagan, T.; Wang, X. Review on Recent Progress in Nitrogen-Doped Graphene: Synthesis, Characterization, and Its Potential Applications. *ACS Catal.* **2012**, *2*, 781−794.
(60) Xu, K.; Fu, Y.; Zhou, Y.; Hennersdorf, F.; Machata, P.; Vincon, I.; Weigand, J. J.; Popov, A. A.; Berger, R.; Feng, X. Cationic Nitrogen-Doped Helical Nanographenes. *Angew. Chem., Int. Ed.* **2017**, *56*, 15876−15881.
(61) Lu, Q.; Greßies, S.; Cembellín, S.; Klauck, F. J. R.; Daniliuc, C. G.; Glorius, F. Redox-Neutral Manganese(I)-Catalyzed C-H Activation: Traceless Directing Group Enabled Regioselective Annulation. *Angew. Chem., Int. Ed.* **2017**, *56*, 12778−12782.
(62) Lu, Q.; Mondal, S.; Cembellín, S.; Greßies, S.; Glorius, F. Site-Selective C-H Activation and Regiospecific Annulation Using Propargylic Carbonates. *Chem. Sci.* **2019**, *10*, 6560−6564.
(63) Seiders, T. J.; Elliott, E. L.; Grube, G. H.; Siegel, J. S. Synthesis of Corannulene and Alkyl Derivatives of Corannulene. *J. Am. Chem. Soc.* **1999**, *121*, 7804−7813.
(64) Sygula, A.; Rabideau, P. W. A Practical, Large Scale Synthesis of the Corannulene System. *J. Am. Chem. Soc.* **2000**, *122*, 6323−6324.
(65) Butterfield, A. M.; Gilomen, B.; Siegel, J. S. Kilogram-Scale Production of Corannulene. *Org. Process Res. Dev.* **2012**, *16*, 664−676.
(66) Matsuoka, W.; Ito, H.; Itami, K. Rapid Access to Nanographenes and Fused Heteroaromatics by Palladium-Catalyzed Annulative π-Extension Reaction of Unfunctionalized Aromatics with Diiodobiaryls. *Angew. Chem., Int. Ed.* **2017**, *56*, 12224−12228.
(67) Koga, Y.; Kaneda, T.; Saito, Y.; Murakami, K.; Itami, K. Synthesis of Partially and Fully Fused Polyaromatics by Annulative Chlorophenylene Dimerization. *Science* **2018**, *359*, 435−439.
(68) Wu, Z. H.; Reichert, H.; Reichelt, H.; Basché, T.; Müllen, K. Photostable NIR-II Pigments from Extended Rylenecarboximides. *Chem.—Eur. J.* **2022**, *28*, No. e202202291.
(69) Ramann, G. A.; Cowen, B. J. Quinoline Synthesis by Improved Skraup-Doebner-Von Miller Reactions Utilizing Acrolein Diethyl Acetal. *Tetrahedron Lett.* **2015**, *56*, 6436−6439.
(70) Yamaguchi, J.; Yamaguchi, A. D.; Itami, K. C-H Bond Functionalization: Emerging Synthetic Tools for Natural Products and Pharmaceuticals. *Angew. Chem., Int. Ed.* **2012**, *51*, 8960−9009.
(71) Kuhl, N.; Hopkinson, M. N.; Wencel-Delord, J.; Glorius, F. Beyond Directing Groups: Transition-Metal-Catalyzed C-H Activation of Simple Arenes. *Angew. Chem., Int. Ed.* **2012**, *51*, 10236−10254.
(72) Dalton, T.; Faber, T.; Glorius, F. C-H Activation: Toward Sustainability and Applications. *ACS Cent. Sci.* **2021**, *7*, 245−261.
(73) Huang, J.; Li, B.; Jiao, P.; Zhong, H. Isoquinoline N-Oxide Synthesis under Pd-Catalysed C-H Activation/Annulation Processes. *Synlett* **2013**, *24*, 2431−2436.
(74) Yu, Q.; Zhang, N.; Huang, J.; Lu, S.; Zhu, Y.; Yu, X.; Zhao, K. Efficient Synthesis of Hydroxyl Isoindolones by a Pd-Mediated C-H

https://doi.org/10.1021/jacsau.4c00105
JACS Au 2024, 4, 1623−1631

Activation/Annulation Reaction. *Chem.—Eur. J.* **2013**, *19*, 11184−11188.
(75) Liu, W.; Yu, Q.; Hu, L.; Chen, Z.; Huang, J. Modular Synthesis of Dihydro-Isoquinolines: Palladium-Catalyzed Sequential C(Sp^2)-H and C(Sp^3)-H Bond Activation. *Chem. Sci.* **2015**, *6*, 5768−5772.
(76) Zhang, G.; Yang, L.; Wang, Y.; Xie, Y.; Huang, H. An Efficient Rh/O_2 Catalytic System for Oxidative C-H Activation/Annulation: Evidence for Rh(I) to Rh(III) Oxidation by Molecular Oxygen. *J. Am. Chem. Soc.* **2013**, *135*, 8850−8853.
(77) Hanson, J. C.; Nordman, C. E. The Crystal and Molecular Structure of Corannulene, $C_{20}H_{10}$. *Acta Crystallogr., Sect. B: Struct. Crystallogr. Cryst. Chem.* **1976**, *32*, 1147−1153.
(78) Haddon, R. C. Chemistry of the Fullerenes: The Manifestation of Strain in a Class of Continuous Aromatic Molecules. *Science* **1993**, *261*, 1545−1550.
(79) Haddon, R. C. Comment on the Relationship of the Pyramidalization Angle at a Conjugated Carbon Atom to the σ Bond Angles. *J. Phys. Chem. A* **2001**, *105*, 4164−4165.
(80) The crystallographic data for corannulene were sourced from the literature (*Acta Crystallogr. B* **1976,** *32,* 1147) and the same calculation process was employed to determine the POAV angles for both **12a**(**2**PF_6^-) and corannulene.
(81) Priyakumar, U. D.; Punnagai, M.; Krishna Mohan, G. P.; Sastry, G. N. A Computational Study of Cation-π Interactions in Polycyclic Systems: Exploring the Dependence on the Curvature and Electronic Factors. *Tetrahedron* **2004**, *60*, 3037−3043.
(82) Greenfield, J. L.; Rizzuto, F. J.; Goldberga, I.; Nitschke, J. R. Self-Assembly of Conjugated Metallopolymers with Tunable Length and Controlled Regiochemistry. *Angew. Chem., Int. Ed.* **2017**, *56*, 7541−7545.
(83) Xie, F.; Finney, N. S. Synthesis and Optical Properties of Mono- and Diaminocorannulenes. *Chem. Commun.* **2020**, *56*, 10525−10528.
(84) Sheldrick, G. M. Crystal Structure Refinement with Shelxl. *Acta Crystallogr., Sect. C: Struct. Chem.* **2015**, *71*, 3−8.
(85) Dolomanov, O. V.; Bourhis, L. J.; Gildea, R. J.; Howard, J. A. K.; Puschmann, H. Olex2: A Complete Structure Solution, Refinement and Analysis Program. *J. Appl. Crystallogr.* **2009**, *42*, 339−341.
(86) Frisch, M. J.; Trucks, G. W.; Schlegel, H. B.; Scuseria, G. E.; Robb, M. A.; Cheeseman, J. R.; Scalmani, G.; Barone, V.; Petersson, G. A.; Nakatsuji, H.; Li, X.; Caricato, M.; Marenich, A. V.; Bloino, J.; Janesko, B. G.; Gomperts, R.; Mennucci, B.; Hratchian, H. P.; Ortiz, J. V.; Izmaylov, A. F.; Sonnenberg, J. L.; Williams-Young, D.; Ding, F.; Lipparini, F.; Egidi, F.; Goings, J.; Peng, B.; Petrone, A.; Henderson, T.; Ranasinghe, D.; Zakrzewski, V. G.; Gao, J.; Rega, N.; Zheng, G.; Liang, W.; Hada, M.; Ehara, M.; Toyota, K.; Fukuda, R.; Hasegawa, J.; Ishida, M.; Nakajima, T.; Honda, Y.; Kitao, O.; Nakai, H.; Vreven, T.; Throssell, K.; Montgomery, J. A.; Peralta, J. E.; Ogliaro, F.; Bearpark, M. J.; Heyd, J. J.; Brothers, E. N.; Kudin, K. N.; Staroverov, V. N.; Keith, T. A.; Kobayashi, R.; Normand, J.; Raghavachari, K.; Rendell, A. P.; Burant, J. C.; Iyengar, S. S.; Tomasi, J.; Cossi, M.; Millam, J. M.; Klene, M.; Adamo, C.; Cammi, R.; Ochterski, J. W.; Martin, R. L.; Morokuma, K.; Farkas, O.; Foresman, J. B.; Fox, D. J. *Gaussian 16*; Gaussian, Inc.: Wallingford, CT, 2016.
(87) Schleyer, P. v. R.; Maerker, C.; Dransfeld, A.; Jiao, H.; van Eikema Hommes, N. J. R. Nucleus-Independent Chemical Shifts: A Simple and Efficient Aromaticity Probe. *J. Am. Chem. Soc.* **1996**, *118*, 6317−6318.
(88) Geuenich, D.; Hess, K.; Köhler, F.; Herges, R. Anisotropy of the Induced Current Density (Acid), a General Method to Quantify and Visualize Electronic Delocalization. *Chem. Rev.* **2005**, *105*, 3758−3772.

https://doi.org/10.1021/jacsau.4c00105
JACS Au 2024, 4, 1623−1631